Cutting force investigation in face milling of additively fabricated nickel alloy 625 via powder bed fusion

Jixiong Fei

Manufacturing and Automation Research Laboratory,
Department of Industrial and Systems Engineering,
Rutgers University,
Piscataway, New Jersey 08854, USA
and
School of Mechanical Engineering,
Tianjin University,
Jinnan, Tianjin 300350, China
Email: tjujackfei@163.com

Guoliang Liu

Manufacturing and Automation Research Laboratory,
Department of Industrial and Systems Engineering,
Rutgers University,
Piscataway, New Jersey 08854, USA
and
School of Mechanical Engineering,
Shandong University,
Jinan, Shandong 250061, China
Email: guoliangone@163.com

Kaushalendra Patel and Tuğrul Özel*

Manufacturing and Automation Research Laboratory,
Department of Industrial and Systems Engineering,
Rutgers University,
Piscataway, New Jersey 08854, USA
Email: kvp44@scarletmail.rutgers.edu
Email: ozel@rutgers.edu
* Corresponding author

Abstract: The face milling of additively fabricated nickel alloy 625 produced via laser powder bed fusion is experimentally investigated. Typically, cutting forces are the most important factor affects the process outcome in terms of surface finish and chatter vibrations in milling of difficult-to-cut materials. The additively fabricated materials possess different mechanical properties hence their cutting force performance is usually unknown. For additively fabricated nickel alloy 625, the build direction and scan strategy rotation are known to influence the resultant workpiece structure with columnar grains. The peak milling force is found dependent upon the feed direction as well as the

layerwise scan rotation employed in fabricating the workpiece. Feeding the cutter against the build direction resulted in lower peak forces with larger deviations, however feeding along the build direction resulted in higher peak forces with lower deviations. The build direction was also observable on fan shaped chip surfaces.

Keywords: additive manufacturing; milling; force; nickel alloy.

Reference to this paper should be made as follows: Fei, J., Liu, G., Patel, K. and Özel, T. (2019) 'Cutting force investigation in face milling of additively fabricated nickel alloy 625 via powder bed fusion', *Int. J. Mechatronics and Manufacturing Systems*, Vol. 12, Nos. 3/4, pp.196–210.

Biographical notes: Jixiong Fei is a visiting PhD student from Tianjin University, China. He received his BE degree in Mechanical Engineering from Tianjin University, China in 2013. He joined the Manufacturing and Automation Research Laboratory at Rutgers University in 2017 and stayed until 2018. His research interests include milling, cutting forces, and additive manufacturing.

Guoliang Liu is a visiting PhD student from Shangdong University, China. He received his BS degree in Mechanical Engineering from Shandong University, China in 2013. He joined the Manufacturing and Automation Research Laboratory at Rutgers University in 2017 and stayed until 2018. His research interests include machining, finite element modeling, and machinability of difficult-to-cut alloys.

Kaushalendra Patel is a graduate student. He received his BTech degree in Mechanical Engineering from Dharmsinh Desai University, India in 2017. He joined the Manufacturing and Automation Research Laboratory at Rutgers University for his graduate studies. His research interests include machining, surface topography and surface quality.

Tuğrul Özel received his PhD in Mechanical Engineering from Ohio State University in 1998, BS degree from Aeronautical Engineering from Istanbul Technical University, Turkey in 1987. He is a Professor at the Industrial and Systems Engineering Department of Rutgers University and the Director of Manufacturing and Automation Research Laboratory (MARL). He has over 150 peer-reviewed journal and conference papers. He serves as the Editor-in-Chief for *International Journal of Mechatronics and Manufacturing Systems*, an Associate Editor for the *ASME Journal of Manufacturing Science and Engineering Control* and a member of several editorial boards of international journals. He is a senior member of ASME and SME.

1 Introduction

Due to their excellent properties, especially retention of strength and hardness at high temperature and good corrosion resistance, titanium and nickel alloys have been widely used in various industries including aerospace, automotive, medical, nuclear, oil and gas. Traditionally, these alloys are first formed as wrought or cast blanks and then rough, semi-finish, and finish machined to their final shape, and their machinability has been a great interest for researchers (Ulutan and Özel, 2011; M'Saoubi et al., 2015). The

machinability of wrought or cast nickel alloys is especially considered difficult and machining induced surface integrity and surface morphology indicate that the microstructure of the machined surface is substantially influenced by tool geometry and tool material, cutting conditions, and lubricating/cooling conditions (Özel and Ulutan, 2012; Jawahir et al., 2011; Arisoy et al., 2016). Especially, the surface integrity is paramount on the machining induced effects on difficult-to-cut materials (Thakur and Gangopadhyay, 2016). Typically, cutting forces are the most important factor affects the process outcome in terms of surface finish and chatter vibrations in milling of difficult-to-cut materials. The additively fabricated materials possess different mechanical properties hence their cutting force performance in multi-axis milling operation is usually unknown and a challenge to practitioners (Calleja et al., 2014).

Additive manufacturing of such alloyed parts from powder material by using directed energy deposition (DED) such as electron beam melting (EBM) and laser powder bed fusion (LPBF) such as selective laser melting (SLM) has been adopted to increase the flexibility and reduce the production cost (Martin et al., 2017; Schmidt et al., 2017). Although a near net shape geometry for additively fabricated parts can be obtained, finish machining processes are still needed to achieve final desired geometry, dimensional tolerances, and surface quality (Wiederkehr and Bergmann, 2018). However, microstructure of additively fabricated alloys is quite different from the wrought or cast counterparts (Trosch et al., 2016). The microstructure of wrought alloys usually contains equiaxed grains after proper heat treatment and the grain size can be considered uniform (Li et al., 2011). On the other hand, there is a columnar grain growth direction typically along the build direction (BD) in additively fabricated alloys and it can also deviate from the build direction (Arisoy et al., 2017; Arisoy et al., 2019). It was found that their microstructure is highly dependent on the BD, and the grain growth is along the BD with a small deviation angle (Deng et al., 2018). It is reported that the yield strength of as-built LPBF nickel alloy 625 samples is about 725 MPa ± 50 MPa in horizontal direction (XY) and is about 615 MPa ± 50 MPa in build direction (Z) respectively. The hardness of as built part is approximately 30 HRC (287 HB) (EOS Nickel alloy IN625 material data sheet, 2019). According to the same reference, Nickel alloy 625 workpieces when fabricated with LPBF can have roughness characteristics as following. As-built surface roughness after shot-peening can have arithmetic mean deviation, Ra, of 4–6.5 μm, and maximum peak-to-valley, Ry, 20–50 μm. This roughness can be reduced to average peak-to-valley profile roughness, Rz, of 0.5 μm after polishing.

It is well acknowledged that the microstructure of workpiece material has significant effects on their machinability. It was suggested that the BD induced microstructure can affect the cutting forces during machining SLM fabricated titanium alloy Ti-6Al-4V when compared against the wrought counterpart (Manikandakumar et al., 2017). Higher cutting forces were observed during turning of SLM manufactured Ti-6Al-4V when the cutting speed was increased.

It was also shown that the SLM manufactured Ti-6Al-4V was more prone to produce segmented chips (Shunmugavel et al., 2019). In another study, the effect of post heat treatment on the machinability of the titanium alloy Ti-6Al-4V manufactured by DED process was investigated (Oyelola et al., 2018). It is reported that the cutting force reduced by 40% under β-annealed condition and 24% under α-annealed condition compared to the as-built DED fabricated Ti-6Al-4V at a low cutting speed, which demonstrated that machinability of the DED manufactured Ti-6Al-4V was severely affected by the change in microstructure induced by the post heat treatment.

The machining induced surface integrity of Ti-6Al-4V manufactured as wrought and additively via EBM and LPBF was also investigated (Rotella et al., 2018). The microstructure and the hardness of the machined surfaces were found to be different from each other. Besides, a thin layer of plastically deformed material with different thicknesses in each case was formed underneath the machined surface.

The machinability of nickel alloy Inconel718 after additive manufacturing was investigated in several studies. A cylindrical shaped nickel alloy Inconel718 bar produced with SLM was used in turning experiments by Kaynak and Tascioglu (2018) when feed rate effect on surface roughness was observed. It was found that increasing feed rate can result in surface work-hardening. The microhardness of machined surface varies with the scan direction and surface integrity can be significantly improved by milling as reported by Brown et al. (2018). Machinability of laser cladding produced Inconel718 alloy was investigated in turning and milling by Calleja et al. (2018). It was reported that cutting forces are higher than usual and lower for laser cladding added material without heat treatment. Tool wear during the milling of SLM-manufactured Inconel718 was investigated by Kim et al. (2018). A lower tool wear was observed in SLM built Inconel 718 when compared to wrought counterpart due to pores and cavities incurred during LPBF, even though the high hardness on the surfaces of the SLM built Inconel718 was measured. Further, the built orientation dominated the re-melted zone in the SLM parts, the contact between the tool and re-melted zone controlled tool wear. They concluded that built orientations should be considered to apply the machining as the post-process.

The literature review shows that the attention was mainly focused on the machinability of additively fabricated titanium alloy Ti-6Al-4V. There is not many work reported on the machinability of additively fabricated nickel alloys. Although research work reported on the machinability of additively fabricated nickel alloy Inconel718, there is no work on nickel alloy 625 which is a solid solution strengthening superalloy in the literature. In this paper, the machinability of the nickel alloy 625 manufactured via LPBF technology was studied by using face milling operations in different cutting directions against the build direction of the workpiece samples.

2 Experimental design

This work is focused on investigating cutting forces in face milling of additively fabricated nickel alloy 625 via laser powder bed fusion. In the experiments, nearly fully dense (relative density of 99%) nickel alloy 625 workpieces with squared top faces (16 mm × 16 mm) and a height of 15 mm were fabricated using the EOS M270 Direct Metal Laser Sintering machine (Criales et al., 2017). In the powder bed, a gas atomized nickel alloy 625 powder (mean particle size of 35 μm and 55% packing density) was used with a fixed layer thickness of s = 20 μm during layerwise additive fabrication process. The parts were built using a laser power of P = 195 W, a scan velocity of v_s = 800 mm/s and a hatch distance of h = 0.10 mm. After nickel alloy 625 workpieces were fabricated by using the LPBF process, the workpieces were removed from the platform by using wire electrical discharge machining and the bottom face and side faces were squared with surface grinding.

The LPBF process involves melting of the powder material and fusing together only the desired locations on the surface of the powder bed. Laser scanning of each layer is

divided up into several bands called stripes that are arranged in various patterns covering the surface. The stripes along the scan direction were processed with the laser beam moving at a constant scan velocity at track by track where weld tracks are separated by a hatch distance. In these test parts, stripes that are 4 mm wide were employed. During the process, stripe patterns were rotated layerwise to attain uniform built. In the tests, two distinct scan strategy rotations (SSR) schemes i.e. orthogonal 90° and 67° layerwise rotation of stripes were considered (Figure 1).

The scan or stripe pattern rotation strategies are known to have distinct effects on the microstructure of the built parts, and as a result their properties are altered (Deng et al., 2018). The previous studies revealed that the microstructure of nickel alloy 625 is influenced by layerwise scan strategy rotation that the growth directions of columnar grains and sizes of cellular grains vary in workpieces built with different rotations (Arisoy et al., 2017). It is also reported that surface roughness of additively built workpieces facing powder bed and as-built surfaces would have higher values as investigated by Özel et al. (2018). Therefore, the face milling experiments were designed and conducted to investigate the effect of directionality and scan strategy rotation related workpiece structures on the machinability.

In the experiments, a vertical milling machine (Tormach CNC 1100), an indexable three-insert toroidal cutter (Tormach TTS M12) which provided a diameter of 25 mm, and carbide round inserts (10 mm diameter) coated with Ti(C,N)+Al_2O_3+TiN (Sandvik R300-1032E-MM 2040) were used. During face milling experiments, the workpiece was fixed on a force dynamometer (Kistler 9121) to measure the cutting forces. The schematic diagram of the experimental setup is shown in Figure 2. Only one insert was mounted on the tool holder. The insert was rotated about 60° to obtain a fresh edge after each cutting test to eliminate inaccuracies that induced by tool wear development. After each cutting experiment, the chips were collected and observed using a digital optical microscope (Nikon Optiphop 100).

Figure 1 Layerwise rotation of stripe patterns during the LPBF process around the build direction (see online version for colours)

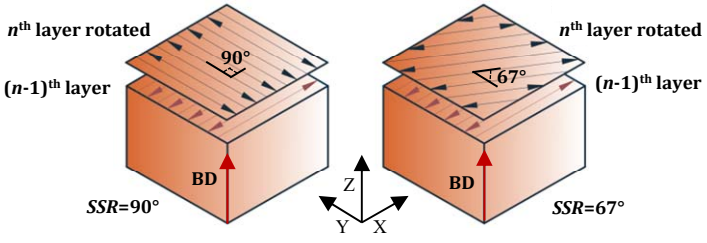

Source: Özel et al. (2018)

The effects of feed direction with respect to the build direction (BD) of the workpiece and the effect of milling force dependent upon the cutting direction as well as the rotating scan direction (SD) used in building the workpiece were investigated. The cutting parameters are listed in Table 1. The axial depth of cut (a_p), radial depth of cut (a_e), and feed rate (v_f) (or feed per tooth, fz) remained unchanged, their values were a_p = 0.1 mm,

a_e = 1.5 mm, f_z = 0.1 mm/tooth, respectively. But the rotational speed (Ω) (or cutting speed, v_c) was varied at three levels.

Table 1 Cutting parameters used in face milling experiments

Test number	*Ω (rpm)*	*v_c (m/min)*	*v_f (mm/min)*
1	636.6	30	63.7
2	1,273	60	127.3
3	1,910	90	191

Figure 2 (a) Schematics of the experimental setup for force measurements in face milling (b) Tool holder with a single round insert installed (see online version for colours)

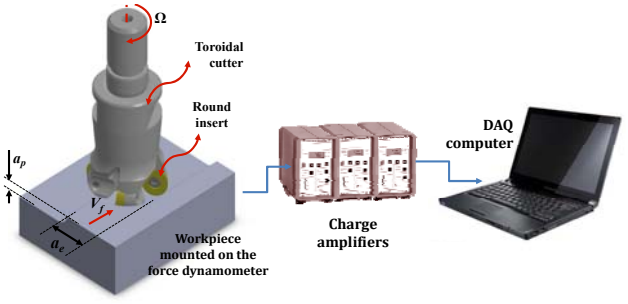

(a)

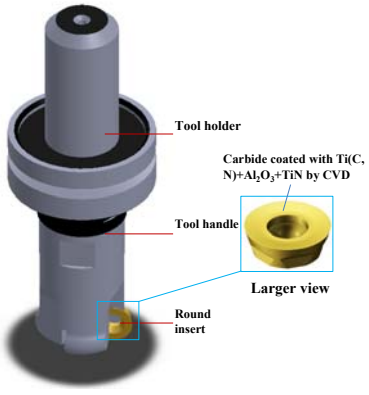

(b)

To investigate the effect of feed direction with respect to faces of the additively fabricated nickel alloy 625 workpieces, face milling along different directions on three different faces were performed. At first, the workpiece was fed along the *y*-direction on the XY face, which is case 1 as indicated in Figure 3. After that, the workpiece was fed along the *x*-direction on the XZ face which is case 2. In case 3, the workpiece was fed along the *z*-direction on the YZ face. All test conditions that are listed in Table 1 were performed for each case of the face milling experiments.

Figure 3 Cutter feed directions at different faces with respect to orthogonally rotating scan direction and build direction (see online version for colours)

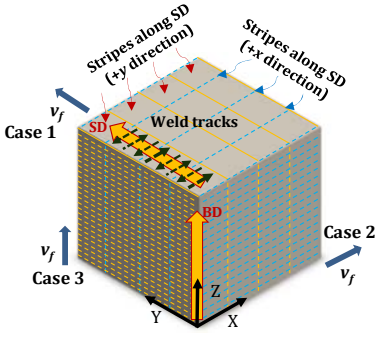

The influence of scan strategy (or stripe pattern) rotation on the machinability of the LPBF nickel alloy 625 was also investigated. Two workpieces with different scan strategy rotations were used in this work; a workpiece built with scan strategy rotation of 90°, and another one built with 67° rotation. Both workpieces were face milled by following climb milling engagement in three cases as indicated in Figure 3.

3 Results and discussion

3.1 Effects of cutting direction on cutting forces

All face milling force signals depict a similar signal form which can be divided into three stages of climb milling cutter engagement, including the stages of cut-in, stable cut, and cut-out as shown in Figure 4(a). At the stage of cut-in, the peak value of milling force in every period keeps increasing, and then decreases to a relatively stable value. When the peak values of milling force generally remain unchanged, the cutting process in this stage is considered stable while in the cut-out stage, the peak value decreases gradually. In this investigation, milling force signals in the stable cut stage as shown in Figure 4(b) are of concern. The peak values of the main milling force at ten periods in the stable cut stages were extracted and then averaged. The averaged peak force value was used in following analysis to investigate the effect of the cutting direction and the scan strategy rotation.

Figure 4 (a) The stages in the milling force signals (b) The force signal with ten periods in the stable range (region 'A') (see online version for colours)

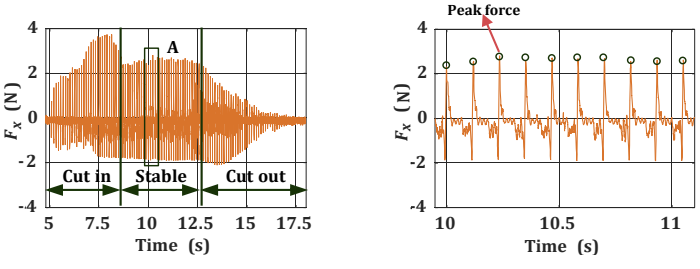

(a) (b)

The averaged cutting force with respect to different cutting directions is shown in Figure 5. The cutting forces for all cutting conditions are normalized by dividing the one obtained at the lowest cutting speed at each case when milling the workpiece sample built with the SSR of 90°. It can be seen from Figure 5 that the main milling forces of case 3 have the largest values in general, while the milling force for cases 1 and 2 almost have same values under the same cutting condition. It should be noted that the error bars on these force graphs represent the standard deviation.

Figure 5 The influence of the cutting direction on the milling forces for the two workpiece samples (see online version for colours)

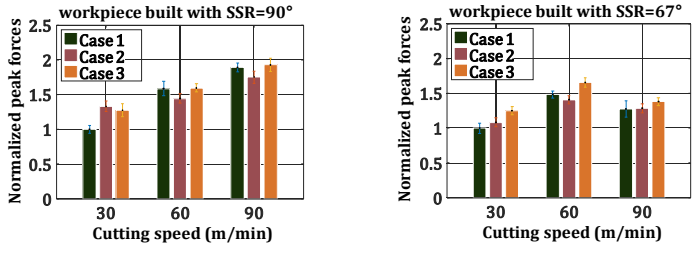

(a) (b)

The cutter was fed against the columnar grains (against BD) in both cases 1 and 2 (as shown in Figure 6), and the cutter sweeps undeformed area and cuts the columnar grains. While for case 3, the cutter was fed along the columnar grain growth direction (along BD). The cutter sweeps mostly the columnar grains and cut the grains. Due to the larger yield strength along the grain growth direction, a higher cutting force is needed to cut the workpiece along the grain growth direction, which means that the milling force in case 3 has the highest values.

Figure 6 The schematics of the relation between the cutting direction, the cutter rotation and the build direction of workpiece samples during face milling at three cases (see online version for colours)

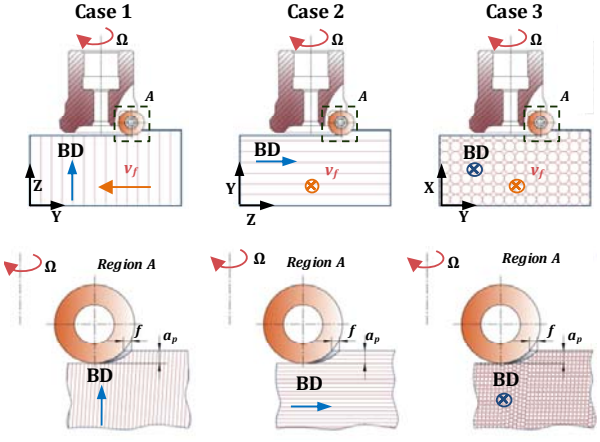

3.2 *Effects of scan strategy rotation on cutting forces*

The normalized average milling forces obtained by cutting two workpiece samples with different scan strategy rotations are also compared, and the comparison results are shown in Figure 7. It can be seen that when milling the workpiece sample built with *SSR* of 67° in all three cases, the main cutting force increased when the cutting speed increased from v_c = 30 m/min to 60 m/min, but decreased when the cutting speed further increased to v_c = 90 m/min. While when milling the workpiece sample built with SSR of 90°, the main cutting force increased steadily when the cutting speed increased from v_c = 30 m/min to 90 m/min. In addition, the main cutting forces of milling the workpiece sample built with SSR of 67° is higher under the cutting speed of v_c = 30 m/min and 60 m/min, but it is lower at the higher cutting speed of v_c = 90 m/min in all three cases. In Figure 7, the standard deviations on the measured peak forces are given as error bars.

The scanning strategy rotation has a significant influence on the microstructure of the built workpiece and mechanical properties (Deng et al., 2018). It was pointed out that the yield strength and the hardness of the additively fabricated workpiece that was built with smaller scan strategy rotation (*SSR* = 45°) have slightly higher values (Ali et al., 2018). Therefore, higher cutting force is needed to remove the workpiece material. That is the primary reason for the cutting forces when milling of the workpiece built with SSR of 67° have higher values when the cutting speeds are v_c = 30 m/min and 60 m/min. Milling force increased with the increasing of cutting speed when increased from v_c = 30 m/min to 60 m/min for both workpiece samples. This is caused by the effect of strain rate

hardening. The strain rate becomes higher in primary deformation zone when the cutting speed is increased. The strain rate hardening also becomes higher during chip formation. When cutting speed increased from v_c = 60 m/min to 90 m/min, cutting forces for the workpiece that was built with SSR of 67° decreased. This may be caused by the thermal softening. An increasing in the cutting speed is generally related to an increase in the cutting temperature and thus the thermal softening of the workpiece. The strain rate hardening is balanced by the thermal softening of the workpiece at the higher cutting speed (v_c = 90 m/min). While for the workpiece that was built with *SSR* of 90°, the cutting force still increased when cutting speed was varied from v_c = 60 m/min to 90 m/min. This means that the strain rate hardening due to a higher cutting speed instead of the thermal softening effect is dominant on the milling forces.

Figure 7 Milling forces comparison between two scan strategies (see online version for colours)

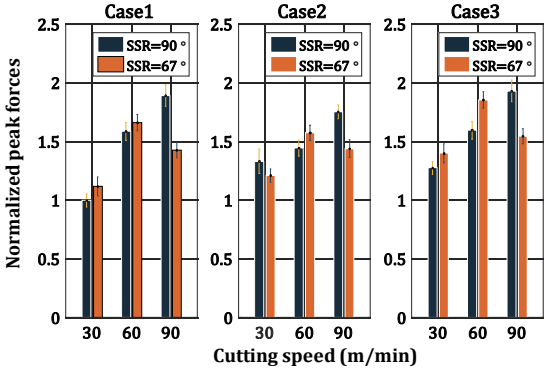

3.3 Effects of scan strategy rotation on chip morphology

The chips collected from experiments were found to have heavily folded fan shapes (see Figure 8). The chips also have saw tooth edges and cracked roots due to interrupted cutting. The chips were slightly curled because of the trochoidal motion of the cutter. The saw tooth edges were mainly observed at the outside end of the chips. The distance between adjacent saw tooth segments is very large. The saw tooth type segmentation occurred for all cutting conditions. Besides, there are cracks at the inner side of the fan-shaped chips. The cracks are either along the radial direction or circumferential direction. At the chip free surface, folds along different directions were observed along the radial direction as shown in Figure 8. It seems that cutting speed and scan strategy rotation has little effect on the chip shapes (Figure 9).

Figure 8 Chip-tool contact surface of the chips (v_c = 90 m/min, f_z = 0.1 mm/tooth, case 1), (a) *SSR* = 90° (b) *SSR* = 67° (see online version for colours)

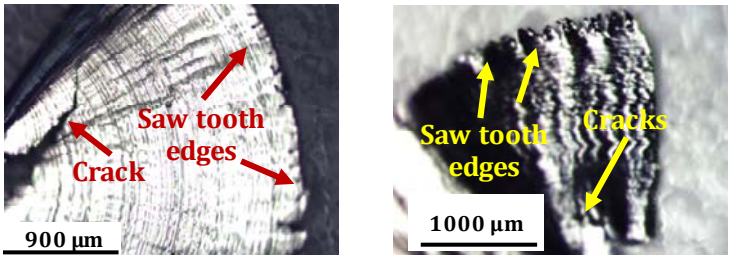

(a) (b)

Two predominant theories to explain the saw tooth chips typically are thermoplastic instability based and the fracture based. The thermoplastic instability theory attributes saw tooth chip morphology to the competition between thermal softening and strain hardening in the shear zone, while the fracture based theory claims that the saw tooth chips are caused by the crack initiation and propagation. However, neither theory can be solely used to explain the saw tooth observed at the ends of the fan-shaped chips. The stress components in the chip can be considered as the stress along the radial direction and the stress along the circumferential direction. The circumferential stress becomes larger and larger as the chip radius increases. At the outer side of the fan shaped chip, the stress is tensile stress. It is large enough to tear the chip repeatedly and thus form the saw tooth edges. At the inner side of the chip, the stress is mainly compressive. It is also large enough to squeeze and buckle the chip and thus leads to cracks on the inner end of the chips.

Figure 9 Free surface of the chips (v_c = 90 m/min, f_z = 0.1 mm/tooth, case 1), (a) *SSR* = 90° (b) *SSR* = 67° (see online version for colours)

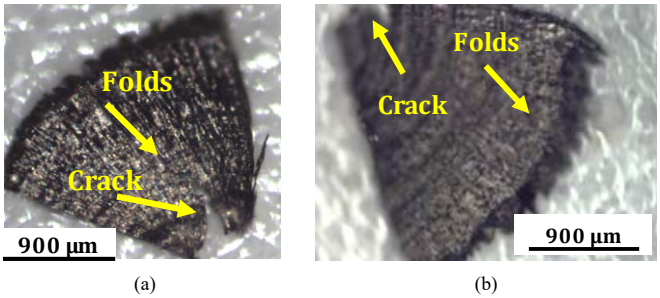

(a) (b)

Figure 10 Surface topography of the face milled nickel alloy 625 fabricated via LPBF (v_c = 90 m/min, f_z = 0.1 mm/tooth, case 1), (a) digital optical image (b) scale-limited surface (c) scale-limited areal surface topography (see online version for colours)

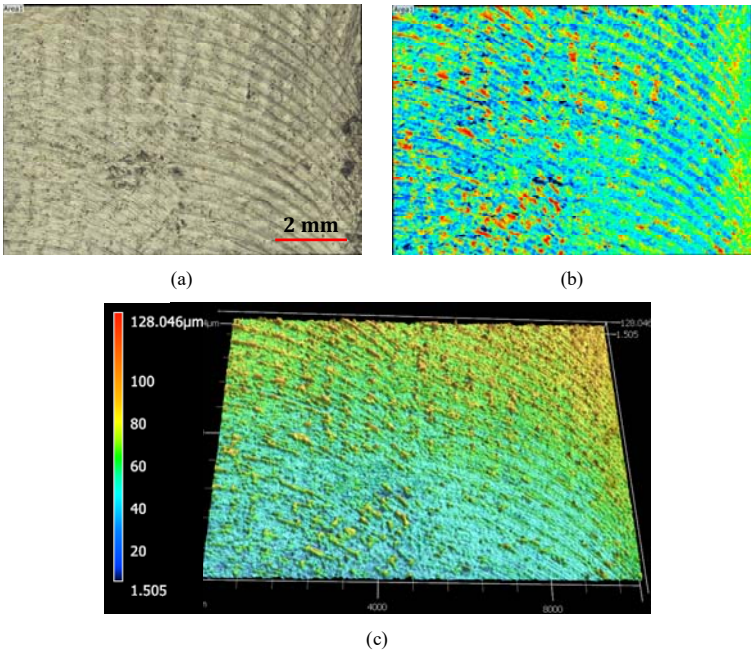

(a) (b)

(c)

The topography of the face milled surfaces reveals very similar characteristics. Figure 10 shows an optical image of the surface area [Figure 10(a)] and a scale-limited height map [Figure 10(b)] obtained by using laser scanning confocal microscopy (Keyence VK-X1000). The scale-limited surface texture parameters are measured as Sa = 6.772 µm, Sq = 9.649 µm (Gaussian filtering conditions, S-filter 8 µm, L-filter 20mm). Based on the surface areal topography, there was a little or no effect of the scan strategy rotation on the surface topography observed.

4 Conclusions

In this paper, the cutting forces generated in the face milling of laser powder bed fusion fabricated nickel alloy 625 are investigated by conducting cutting experiments in different workpiece orientations and using a single round insert cutter. The effects of the cutting direction and layer-by-layer scan strategy rotation on the peak milling force and chip morphology are discussed. The effect of increasing the cutting speed is reported. It was observed that the milling forces are different when cutting additively fabricated

workpiece in different orientations. The results analyzed from the milling experiments lead to following specific conclusions:

- Cutting along the BD or normal to the BD will have influence on the milling force, cutting force has the highest value when feeding along the columnar grain growth direction.
- The scanning strategy will affect the milling force because it has an effect on the physical parameters and the microstructure of the additively manufactured workpiece, and thus the milling force.
- The chips generated in face milling are discontinuous and have a fan shape. Saw teeth mainly exist at the outside end of the fan shaped chips.
- The cracks observed exist on the inner side of fan shaped chips and most of the cracks are along the radial direction of the fan shaped chips while a few of them are along the circumferential direction.
- There is no observable effect on surface topography.

References

Ali, H., Ghadbeigi, H. and Mumtaz, K. (2018) 'Effect of scanning strategies on residual stress and mechanical properties of selective laser melted Ti6Al4V', *Materials Science and Engineering: A*, Vol. 712, pp.175–187.

Arisoy, Y.M., Criales, L.E. and Özel, T. (2019) 'Modeling and simulation of thermal field and solidification in laser powder bed fusion of nickel alloy IN625', *Optics and Laser Technology*, Vol. 109, pp.278–292.

Arisoy, Y.M., Criales, L.E., Özel, T., Lane, B., Moylan, S. and Donmez, A. (2017) 'Influence of scan strategy and process parameters on microstructure and its optimization in additively manufactured nickel alloy 625 via laser powder bed fusion', *International Journal of Advanced Manufacturing Technology*, Vol. 90, Nos. 5–8, pp.1393–1417.

Arisoy, Y.M., Guo, C., Kaftanoğlu, B. and Özel, T. (2016) 'Investigations on microstructural changes in machining of Inconel 100 alloy using face turning experiments and 3D finite element simulations', *International Journal of Mechanical Sciences*, Vol. 107, pp.80–92.

Brown, D., Li, C., Liu, Z.Y., Fang, X.Y. and Guo, Y.B. (2018) 'Surface integrity of Inconel 718 by hybrid selective laser melting and milling', *Journal of Virtual and Physical Prototyping*, Vol. 13, No. 1, pp.26–31.

Calleja, A., Tabernero, I., Ander, J., Francisco, E., Campa, J., Lamikiz, A. and de Lacalle, L.N.L. (2014) 'Feed rate calculation algorithm for the homogeneous material deposition of blisk blades by 5-axis laser cladding', *International Journal of Advanced Manufacturing Technology*, Vol. 74, Nos. 9–12, pp.1219–1228.

Calleja, A., Urbikain, G., González, H., Cerrillo, I., Polvorosa, R. and Lamikiz, A. (2018) 'Inconel®718 superalloy machinability evaluation after laser cladding additive manufacturing process', *International Journal of Advanced Manufacturing Technology*, Vol. 97, Nos. 5–8, pp.2873–2885.

Criales, L.E., Arısoy, Y.M., Lane, B., Moylan, S., Donmez, A. and Özel, T. (2017) 'Laser powder bed fusion of nickel alloy 625: experimental investigations of effects of process parameters on melt pool size and shape with spatter analysis', *International Journal of Machine Tools and Manufacture*, Vol. 121, pp.22–36.

Deng, D., Peng, R.L., Brodin, H. and Moverare, J. (2018) 'Microstructure and mechanical properties of Inconel 718 produced by selective laser melting: sample orientation dependence and effects of post heat treatments', *Materials Science and Engineering: A*, Vol. 713, pp.294–306.

EOS Nickel Alloy IN625 Material Data Sheet [online] https://dmlstechnology.com/images/pdf/EOS_NickelAlloy_IN625.pdf (accessed 29 May 2019).

Jawahir, I.S., Brinksmeier, E., M'Saoubi, R., Aspinwall, D.K., Outeiro, J.C., Meyer, D., Umbrello, D. and Jayal, A.D. (2011) 'Surface integrity in material removal processes: recent advances', *CIRP Annals – Manufacturing Technology*, Vol. 60, No. 2, pp.603–626.

Kaynak, Y. and Tascioglu, E. (2018) 'Finish machining-induced surface roughness, microhardness and XRD analysis of selective laser melted Inconel 718 alloy', *Procedia CIRP*, Vol. 71, pp.500–504.

Kim, D., Park, E., Kim, N. and Park, H., (2018) 'Experimental investigation on tool wear during the milling processes for the post-processing of selective laser melted Inconel 718 alloys', *ASME International Manufacturing Science and Engineering Conference*, Paper No. MSEC2018-6561, V001T01A011, doi: 10.1115/MSEC2018-6561.

Li, D., Guo, Q., Guo, S., Peng, H. and Wu, Z. (2011) 'The microstructure evolution and nucleation mechanisms of dynamic recrystallization in hot-deformed Inconel 625 superalloy', *Materials and Design*, Vol. 32, pp.696–705.

M'Saoubi, R., Axinte, D., Soo, S.L., Nobel, C., Attia, H., Kappmeyer, G., Engin, S. and Sim, W-M. (2015) 'High performance cutting of advanced aerospace alloys and composite materials', *CIRP Annals – Manufacturing Technology*, Vol. 64, No. 2, pp.557–580.

Manikandakumar, S., Ashwin, P., Moshe, G., Rajkumar, S. and Guy, L. (2017) 'A comparative study of mechanical properties and machinability of wrought and additive manufactured (selective laser melting) titanium alloy-Ti-6Al-4V', *Rapid Prototyping Journal*, Vol. 23, No. 6, pp.1051–1056.

Martin, J.H., Yahata, B.D., Hundley, J.M., Mayer, J.A., Schaedler, T.A. and Pollock, T.M. (2017) '3D printing of high-strength aluminium alloys', *Nature*, Vol. 549, pp.365–369.

Oyelola, O., Crawforth, P., M'Saoubi, R. and Clare, A.T. (2018) 'On the machinability of directed energy deposited Ti6Al4V', *Additive Manufacturing*, Vol. 19, pp.39–50.

Özel, T. and Ulutan, D. (2012) 'Prediction of machining induced residual stresses in turning of titanium and nickel based alloys with experiments and finite element simulations', *CIRP Annals – Manufacturing Technology*, Vol. 61, No. 1, pp.547–550.

Özel, T., Altay, A., Donmez, A. and Leach, R. (2018) 'Surface topography investigations on nickel alloy 625 fabricated via laser powder bed fusion', *International Journal of Advanced Manufacturing Technology*, Vol. 94, Nos. 9–12, pp 4451–4458.

Rotella, G., Imbrogno, S., Candamano, S. and Umbrello, D. (2018) 'Surface integrity of machined additively manufactured Ti alloys', *Journal of Materials Processing Technology*', Vol. 259, pp.180–185.

Schmidt, M., Merklein, M., Bourell, D., Dimitrov, D., Hausotte, T., Wegener, K., Overmeyer, L., Vollertsen, F. and Levy, G.N. (2017) 'Laser based additive manufacturing in industry and academia', *CIRP Annals – Manufacturing Technology*, Vol. 66, No. 2, pp.561–583.

Shunmugavel, M., Goldberg, M., Polishetty, A., Nomani, J., Sun, S. and Littlefair, G. (2019) 'Chip formation characteristics of selective laser melted Ti-6Al-4V', *Australian Journal of Mechanical Engineering*, Vol. 17, No. 2, pp.109–126.

Thakur, A. and Gangopadhyay, S. (2016) 'State-of-the-art in surface integrity in machining of nickel-based super alloys', *International Journal of Machine Tools and Manufacture*, Vol. 100, pp.25–54.

Trosch, T., Strößner, J., Völkl, R. and Glatzel, U. (2016) 'Microstructure and mechanical properties of selective laser melted Inconel 718 compared to forging and casting', *Materials Letters*, Vol. 164, pp.428–431.

Ulutan, D. and Özel, T. (2011) 'Machining induced surface integrity in titanium and nickel alloys: a review', *International Journal of Machine Tools and Manufacture*, Vol. 51, No. 3, pp.250–280.

Wiederkehr, P. and Bergmann, J.A. (2018) 'An integrated macroscopic model for simulating SLM and milling processes', *Production Engineering*, Vol. 12, No. 3–4, pp 465–472.